Thermal and vibrational-state selected rates of the $CH_4+Cl \leftrightarrow HCl+CH_3$ reaction

Wendell T. Duncan and Thanh N. Truong

Department of Chemistry, University of Utah, Salt Lake City, Utah 84112

We present direct *ab initio* dynamics studies of thermal and vibrational-state selected rates of the hydrogen abstraction $CH_4+Cl \leftrightarrow CH_3+HCl$ reaction. Rate constants were calculated within the canonical variational transition state theory formalism augmented by multidimensional semiclassical tunneling corrections. A vibrational diabatic model was used for vibrational-state selected rate calculations, particularly for exciting the CH_4 symmetric stretching and umbrella bending modes. The potential energy information was calculated by a combined density functional and molecular orbital approach. Becke's half-and-half (BH&H) nonlocal exchange and Lee–Yang–Parr (LYP) nonlocal correlation functionals (BH&HLYP) were used with the $6\text{-}311G(d,p)$ basis set for determining structures and frequencies at the stationary points and along the minimum energy path (MEP). Energetics information was further improved by a series of single point spin-projected fourth-order Møller–Plesset perturbation theory (PMP4(SDTQ)) calculations using the $6\text{-}311+G(2df,2pd)$ basis set. We found that the calculated thermal rate constants have reasonable agreement with experimental results for both the forward and reverse reactions. Our results also predict that exciting the CH_4 symmetric stretching mode will greatly enhance the hydrogen atom transfer rate. Surprisingly, exciting the CH_4 umbrella bend mode is also predicted to have a noticeable enhancement factor at room temperature. © *1995 American Institute of Physics.*

I. INTRODUCTION

The $CH_4+Cl \leftrightarrow HCl+CH_3$ reaction has been a focus of many kinetic experiments[1–14] due to its importance to atmospheric chemistry, the role of chlorine in catalyzing methane to ethane, and basic understanding of hydrocarbon halogenation reactions. In particular, it is a one of the major sinks of Cl radicals in the catalytic reaction of ozone in the earth's atmosphere. Theoretical studies of this reaction, however, have been limited. Previous *ab initio* studies[15–18] have provided structural and energetic information at the stationary points and in the vicinity of the transition state. Thermal rate constants were also calculated by using conventional transition state theory with Wigner tunneling corrections (TST/W)[19] or interpolated TST with Eckart tunneling corrections.[20] For the reverse reaction, TST/W and RRKM theory were used to calculate the rate constants.[18] The recent study by Dobbs and Dixon[17] reported accurate *ab initio* molecular orbital (MO) as well as density functional theory (DFT) calculations. They concluded that nonlocal DFT methods, particularly the BLYP and B3LYP methods, which are the combinations of Becke88's[21] or Becke's three-parameter exchange[22] with the Lee–Yang–Parr correlation[23] functionals, give poor transition state properties. In our previous studies,[24–26] we found that the Becke's half-and-half BH&H[27] exchange with LYP correlation functionals, which were not included in Dobbs and Dixon's study, can provide accurate information on transition state properties, particularly geometries and frequencies.

From a more fundamental point of view, the abstraction reaction $Cl+CH_4$ poses particularly interesting questions regarding its detailed dynamics. First, it has similar reaction kinematics to the atom–diatom heavy–light–heavy $Cl+HCl$ reaction.[28,29] In particular, both have similar relative translational reduced mass and skew angle, and proceed with substantial forward barriers. The main difference is in the dimensionality of the potential energy surface, 18 degrees of freedom for the $Cl+CH_4$ vs 9 for the $Cl+HCl$ reaction. It is of particular interest to understand how such an increase in the dimensionality of the potential energy surface manifests itself in the detailed dynamics of the atom+polyatom $Cl+CH_4$ reaction as compared to the well-understood atom–diatom $Cl+HCl$ reaction. The $Cl+CH_4$ reaction is slightly endothermic. The propensity rule[30] for gas-phase atom–diatom reactions would suggest that vibrational energy is more effective than translational energy in promoting the endothermic reaction. If such a propensity rule applies to atom–polyatom reactions, which of the four CH_4 vibrational modes would be active? Experimental investigations on the effects of reagent vibrational excitation on dynamics of polyatomic bimolecular reactions often face considerable challenges. Theory can be a valuable partner by providing information on the potential energy surface and insights into these effects. The main focus of our present study is to provide potential energy information and predictions on the effects of excitation of different CH_4 vibrations on the dynamics of the $Cl+CH_4$ reaction. Experimental studies on state-specific rates of this reaction are being carried out by Zare and co-workers.[31]

The detailed state-specific dynamics of polyatomic bimolecular reactions poses a considerable challenge to theory. The size of the system considered here precludes any quantum dynamics considerations. Semiclassical trajectory calculations could provide detailed pictures of the dynamics. However, such calculations depend on the availability of an accurate analytical potential energy function which does not exist in the foreseeable future. Developing a new potential energy function for this reaction is time consuming and is not

a trivial task. The direct dynamics approach,[24–26] where the potential energy information required for dynamical calculations is calculated directly from electronic structure theory offers a viable alternative for studying the dynamics of this reaction. Note that structural, energetic, and frequency information of the reactants and transition state is sufficient for conventional transition state theory calculations. However, previous studies[32] have pointed out that conventional transition state theory grossly overestimates the vibrational-state selected rate enhancement factor. In our previous *ab initio* dynamics study on vibrational-state selected rates of the OH(v)+H$_2$(v') reaction,[26] we found that the reaction path Hamiltonian approach, where structural, energetic and frequency information along the minimum energy path (MEP) is required, yields good agreement with experimental data on the enhancement factors due to excitation of either the OH or H$_2$ stretching mode. Even with this direct dynamics approach, the number of electrons in the Cl+CH$_4$ system would still pose a computational challenge if such information were to be computed at a sufficiently accurate level of *ab initio* molecular orbital theory. Recently, we have proposed a computationally less demanding direct *ab initio* dynamics approach.[24] In particular, a nonlocal DFT method is used to calculate the structural and frequency information along the MEP, which is the computationally most demanding step. The energy along the MEP is corrected by performing a series of single point calculations at a more accurate level of *ab initio* MO theory. This approach has been found to give accurate thermal rate constants for the bimolecular H+CH$_4$↔CH$_3$+H$_2$ reaction[24] and the unimolecular water-assisted tautomerization reaction in formamidine–water complexes.[25] Another approach would use the semiempirical molecular orbital theory at the neglected-diatomic-differential-overlap level where the parameters are fitted to accurate *ab initio* calculations or experimental data for a specific reaction.[33–37]

In the present study, we use our combined DFT/*ab initio* MO direct dynamics approach to calculate both the thermal and vibrational-state selected rate constants for the Cl+CH$_4$ reaction for a wide range of temperatures. Rate constants were calculated using variational transition state theory (VTST)[32,38,39] with corrections for multidimensional semiclassical tunneling[40] and spin–orbit coupling effects. For vibrational-state selected reactions, we employed the vibrationally diabatic model that was introduced by Truhlar and Isaacson[41] and was successfully employed in our previous study of the OH(v)+H$_2$(v') reaction.[26] We discuss briefly the underlying theory in Sec. II. The computational details are discussed in Sec. III. Results and discussion are given in Section IV.

II. THEORY

For a canonical ensemble, the variational TST (CVT) thermal rate constants for a gas-phase bimolecular reaction is determined by varying the location of the dividing surface along the reaction coordinate s to minimize the generalized TST rate constants, $k^{GT}(T,s)$. Thus, the CVT thermal rate constant, k^{CVT}, at the temperature T is given by

$$k^{CVT}(T) = \min_{s} \{k^{GT}(T,s)\}$$

$$= \min_{s} \left\{ \sigma \frac{k_b T}{h} \frac{Q^{GT}(T,s)}{Q^R(T)} e^{-V_{MEP}(s)/k_b T} \right\}, \quad (1)$$

where Q^{GT} is the internal partition function of the generalized transition state with the local zero of energy at $V_{MEP}(s)$, which is the classical potential energy along the minimum energy path (MEP); Q^R is the reactant partition function per unit volume; σ is the symmetry factor, which is 4 for the forward and 2 for the reverse direction of the Cl+CH$_4$↔CH$_3$+HCl reaction; k_b and h are the Boltzmann and Planck constants, respectively. The MEP is defined as the steepest descent path, in the mass-weighted Cartesian coordinates, on the Born–Oppenheimer potential energy surface from the transition state to both the reactants and products. Q^{GT} and Q^R are approximated as products of electronic, rotational, and vibrational partition functions. For Q^R, the relative translational partition function is also included. Translational and rotational partition functions were evaluated classically whereas the vibrational partition functions were calculated quantum mechanically within the harmonic approximation.

The spin–orbit coupling effects on the reaction rates are considered statistically. The $^2P_{1/2}$ and $^2P_{3/2}$ states of the Cl atom, with splitting of 882 cm^{-1}, are included in the calculations of the Cl electronic partition function. Furthermore the $^2P_{3/2}$ state is stabilized by 294 cm^{-1}, thus the spin–orbit coupling effectively raises the barrier by the same amount which is included in our calculation of the rate constants. The statistical approach was found to be reasonably accurate for the Cl+HCl reaction.[42]

For vibrational-state selected rate constants, we employ a statistical vibrationally diabatic model[41] which assumes that vibrational modes preserve their characteristic motions along the reaction coordinate. In this case, vibrational modes were correlated by maximizing the overlap of successive points on the reaction coordinate. Within this statistical–diabatic model, the CVT expression for vibrational-state selected rate constants differs from the statistical form of the thermal rate only in the vibrational partition function for the selected mode. In particular, the vibrational partition of mode i in state m is given by

$$q_i(m,T) = e^{-(1/2+m)\hbar w_i/k_b T}. \quad (2)$$

In the CVT rate, the motion along the reaction coordinate is still treated classically. Tunneling along this degree of freedom is included by a transmission coefficient. In this study, the effective (diabatic) potential for tunneling in the vibrational-state selected reaction is defined by

$$V_d(\{m_i\},s) = V_{MEP}(s) + \sum_{i=1}^{3N-7} \left(\frac{1}{2} + m_i \right) \hbar w_i(s), \quad (3)$$

where m_i is the vibrational state of mode i and 3N-7 is the number of generalized frequencies for the nonlinear N-atom polyatomic system. In Eq. (3), modes that do not correlate to the reactant vibrations are assumed to be in the ground state. For thermal rate calculations, the effective potential for tun-

neling is the vibrational adiabatic ground-state potential, which has the same form as in Eq. (3) but all vibrational modes are in the ground states. The transmission coefficients were calculated with multidimensional semiclassical zero- and small-curvature tunneling methods, denoted as ZCT and SCT, respectively. The SCT transmission coefficients, that include the reaction-path curvature effect on the transmission probability, were based on the centrifugal-dominant small curvature semiclassical adiabatic ground-state (CD-SCSAG) approximation[40] with our recent modifications[26] applied to the vibrational-state selected case. In particular, the transmission probability at energy E is given by

$$P(E) = \frac{1}{\{1 + e^{-2\theta(E)}\}}, \qquad (4)$$

where $\theta(E)$ is the imaginary action integral evaluated along the reaction coordinate

$$\theta(E) = \frac{2\pi}{h} \int_{s_l}^{s_r} \sqrt{2\mu_{\text{eff}}(s)|E - V_d(s)|}\,ds, \qquad (5)$$

and where the integration limits s_l and s_r are the reaction coordinate classical turning points. The reaction-path curvature effect on the tunneling probability is included in the effective reduced mass, μ_{eff}. Thus, the ZCT transmission coefficients can be obtained by setting μ_{eff} equal to μ in Eq. (5). More details on the VTST and tunneling methods can be found elsewhere.[32,38–40]

III. COMPUTATIONAL DETAILS

A. Electronic structure

Optimized geometries and frequencies of CH_4, CH_3, HCl, the $H_3C\cdots HCl$ complex, and $H3C\cdots H\cdots Cl$ transition state were determined at both the BH&HLYP and quadratic configuration interaction (QCISD), which includes all single and double excitations, levels of theory using a split valence triple zeta basis set augmented by a set of d functions for C and Cl and a set of p functions for H, namely the 6-311G(d,p) basis set. Nearly identical results were ob-

tained at the stationary points if the MC-311G(d,p) basis set was used (results are not included here). Note that the 6-311G basis set was found to have certain deficiencies in the s and p valence orbital portions.[43] A more accurate basis set such as from the correlation consistent basis sets[44–46] would be more desired, however, it was not considered in this study. We have tested the BLYP, B3LYP, and BP nonlocal DFT methods, but were either unable to find or found very poor transition state structures. These results are not included here and will not be discussed further in this study. In our experience, the BH&HLYP method as implemented in the GAUSSIAN 92/DFT programs[47] appears to give better results for open-shell transition state structures than other DFT methods. It should be noted that this implementation of the BH&H exchange functional is different from that originally proposed by Becke. The amount of Hartree–Fock exchange mixing was determined from a fitting procedure with no formal basis. However, such a mixing of HF exchange in a similar approach was found to be important for calculating transition state properties.[48] Furthermore, as discussed below, this method seems to work well for the Cl+CH_4 reaction by comparing to the results from the present QCISD and previous MO calculations. The MEP was calculated in mass-weighted internal coordinates with the small step size of 0.01 amu$^{1/2}$ bohr using the Gonzalez–Schlegel method.[49] It has been found that this method yields nearly identical MEP's for integrating in the mass-weighted internal and mass-weighted Cartesian coordinates. Also the correct curvature vectors in the limit of small step size are produced.[49] Hessians at selected points along the MEP needed for CVT calculations were chosen according to the focusing technique described below. To improve the energetic information, single point spin-projected fourth-order Møller–Plesset perturbation theory (PMP4(SDTQ))[50] calculations at the BH&HLYP geometries using a much larger basis set, namely the 6-311+G$(2df,2pd)$ basis set, were carried out at the Hessian grid points. UMP4(SDTQ)[51] results at the stationary points are also presented for comparison.

TABLE I. Calculated and experimental geometrical parameters (distances in Å, angle in degrees) at the stationary points.

		BH&HLYP[a]	QCISD[a]	MP-SAC2[b]	MP2(FU)[c]	Expt.[d]
HCl	R_{HH}	1.276	1.276	1.276	1.276	1.275
CH_3	R_{CH}	1.073	1.083	1.080	1.072	1.079
CH_4	R_{HH}	1.084	1.093	1.090	1.083	1.091±0.002
$H_3C\cdots H\cdots Cl$	R_{CH}	1.443	1.404	1.431	1.375	
T.S.	$R_{CH'}$	1.077	1.088	1.086	1.078	
	R_{HCl}	1.431	1.443	1.388	1.452	
	$\angle_{HCH'}$	100.6	101.6	101.2	101.2	
$CH_3\cdots HCl$	R_{CH}	2.248			2.337	
Complex	$R_{CH'}$	1.074			1.080	
	R_{HCl}	1.288			1.287	
	$\angle_{HCH'}$	93.6			94.3	

[a]Calculated using the 6-311G(d,p) basis set.
[b]Results from Truong et al. using the MC-311G$(2d,d,p)$ basis set (Ref. 15).
[c]Results from Dobbs and Dixon using the TZ+2P basis set (Ref. 17) except for the complex that are taken from Chen et al. (Ref. 16).
[d]From Ref. 9.

TABLE II. Calculated and experimental frequencies (cm^{-1}) at the stationary points.

	Symmetry	BH&HLYP	QCISD	MP2(FU)[a]	Expt.[b]
HCl		3059	3045	3063	2991
CH_3	a_1'	3187	3127	3178	3002
	a_2''	500	433	460	580
	e'	3370	3309	3369	3184
	e'	1453	1436	1441	1383
CH_4	a_1	3107	3046	3076	2917
	e	1609	1573	1591	1534
	t_2	3217	3166	3212	3019
	t_2	1389	1367	1369	1306
$H_3C\cdots HCl$	$\nu_1\ a_1$	3180		3209	
Complex	ν_2	2887		2930	
	ν_3	658		630	
	ν_4	97		100	
	$\nu_5\ e$	3364		3397	
	ν_6	1455		1481	
	ν_7	359		328	
	ν_8	160		142	
$H_3C\cdots H\cdots Cl$	$\nu_1\ a_1$	3162	3100	3132	
T.S.	ν_2	1211	1207	1213	
	ν_3	541	505	511	
	$\nu_4\ e$	3328	3259	3305	
	ν_5	1468	1449	1448	
	ν_6	920	939	958	
	ν_7	385	355	378	
	$\nu_8\ a_1$	996i	1228i	1262i	

[a]Values are taken from Dobbs and Dixon (Ref. 17) except for the complex that are taken from Chen *et al.* (Ref. 16).
[b]Taken from Ref. 54.

All electronic structure calculations were done using the GAUSSIAN92/DFT program.[47]

B. Rate calculations

A focusing technique or an adaptive mesh method proposed in our previous study[25,52] was used to obtain the optimum accuracy in the calculated rate constants for a given resource. This was done by first screening the reaction valley with a coarse grid to locate regions that are most sensitive to the dynamics of the $Cl+CH_4$ reaction then using a finer grid just for these regions. For state-selected rate constants, we found that additional Hessians far from the transition state

region are also needed. Thermal and vibrational-state selected rate constants were calculated by using our DiRate (Direct Rate) program.[53]

IV. RESULTS AND DISCUSSION

In our previous studies,[24,25] we have found that the BH&HLYP method yields accurate frequencies and geometries along the MEP. However, it is necessary to verify such a conclusion for the $Cl+CH_4$ reaction prior to rate calculations. For this reason, in addition to the discussion of features on the potential energy surface of the $Cl+CH_4$ system, we also discuss the accuracy of the BH&HLYP method by comparing it to accurate *ab initio* MO results.

A. Reactants, products and transition state

1. Geometries

Geometrical parameters for the stationary points obtained from different theoretical methods are listed in Table I along with available experimental data. For the reactant and product structures, namely, HCl, CH_4, and CH_3 molecules, the BH&HLYP method yields excellent agreement with the experimental data. The largest difference in the bond length is on the order of 0.007 Å. Similar agreement is also found when comparing the *ab initio* results from QCSID, MP2-SAC,[15] and MP2(FU)[17] calculations with the experimental data. The largest discrepancies between calculated geometries are found at the transition state, particularly for the active CH and HCl bonds, i.e., bonds that are either forming or breaking. The BH&HLYP method predicts these CH and HCl bond distances to be 1.443 and 1.431 Å, respectively, as compared to 1.375 and 1.452 Å from previous MP2/TZ+2P calculations.[17] Slightly worse agreement is observed when comparing to more accurate *ab initio* results from our present QCISD calculations.

An interesting point is the existence of a loosely bound complex discovered by Chen *et al.*[16] using G1 theory. These authors found that the C_{3v} complex is stabilized by 0.627 kcal/mol when the HCl molecule is 2.337 Å away from the CH_3 radical. In our present study, we found this complex lies 2.32 kcal/mol below the separated products at both the BH&HLYP and the PMP4//BH&HLYP levels. We were unable to find a stable complex at the QCISD level with the 6-311G(d,p) basis set. At the BH&HLYP level, the

TABLE III. Reaction energies and barrier heights (kcal/mol) of the $CH_4+Cl\rightarrow CH_3+HCl$ reaction.

	BH&HLYP[a]	QCISD[a]	PMP4//DFT[b]	MP4//DFT[c]	MP-SAC2[d]	CCSD(T)//MP2[e]
ΔE	8.95	9.85	6.38(6.4)[f]	6.52	6.7	6.85
ΔH	3.58	4.56	1.02	1.63	1.2	1.91
$\Delta V_f^\ddagger$	9.87	14.0	7.87	8.86	7.9	8.96
$\Delta V_{a,f}^{G\ddagger}$	5.54	9.77	3.55	4.53	3.5	4.93
$\Delta V_r^\ddagger$	0.92	4.18	1.50	2.32	1.2	2.11
$\Delta V_{a,r}^{G\ddagger}$	1.96	5.21	2.53	3.37	2.3	3.02

[a]Calculated using the 6-311G(d,p) basis set.
[b]Single point PMP4(SDTQ)/6-311+G($2df,2pd$) energy calculations at the BH&HLYP/6-311G(d,p) geometries.
[c]Single point MP4(SDTQ)/6-311+G($2df,2pd$) energy calculations at the BH&HLYP/6-311G(d,p) geometries.
[d]Results from Truong *et al.* (Ref. 15) using the MC-311G($2d,d,p$) basis set.
[e]Single point CCSD(T)/CC-pVQZ(no g) energy calculations at the MP2/TZ+2p geometries from Dobbs and Dixon (Ref. 17).
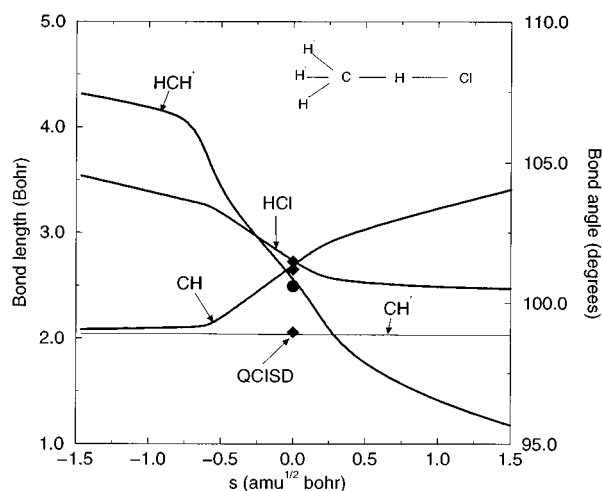[f]Value in the parentheses is the experimental estimate from the binding energies. Taken from Ref. 15.

FIG. 1. Geometrical parameters plotted vs the reaction coordinate s. Curves are results from BH&HLYP/6-311G(d,p) calculations. Diamonds are QCISD/6-311G(d,p) bond lengths and circle is the angle at the transition state.

FIG. 3. Classical potential energy along the minimum energy path. Solid line is the BH&HLYP/6-311G(d,p) results and the dashed line is from single point MP4/6-311+G($2df,2pd$)//BH&HLYP/6-311G(d,p) calculations. Diamond is CCSD(T)/CC-pVQZ(no g)//MP2/TZ+2p calculated barrier (Ref. 17).

$H_3C...HCL$ complex has C_{3v} symmetry, and a linear C–H–Cl structure, with a complex separation distance of 2.248 Å. Note that the existence of such a complex would affect the product rotational distributions in molecular beam experiments, however it does not affect the rate constants of the Cl+CH_4 reaction calculated in this study.

2. Frequencies

Calculated harmonic frequencies at the stationary points are listed in Table II along with the experimental data[54] for CH_4, CH_3, and HCl molecules. The calculated BH&HLYP frequencies for CH_4, CH_3, and HCl molecules agree very well with the experimental values, with the largest error be-
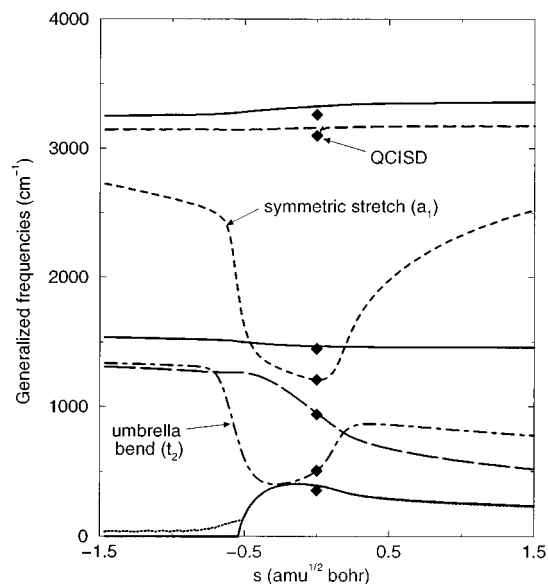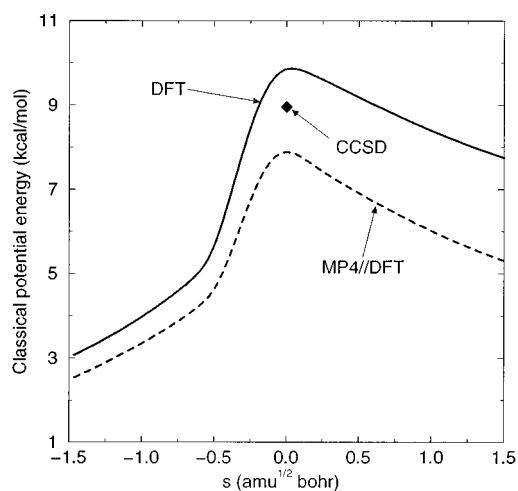
ing 13.8% for the low-frequency umbrella bending mode of CH_3. All other modes have errors less than 6.5%. Similar agreement between BH&HLYP and QCISD theories for the stable structures is also found with differences on the order of 2.0% except for the CH_3 umbrella bending mode for which the DFT method produces a better result than QCISD results. The transition state frequencies for bound modes calculated at the BH&HLYP level differ respectively from our QCISD and MP2 results by at most 8.4% and 5.9% with the largest differences of 30 and 30 cm^{-1} occurring for low-frequency modes. This is quite encouraging since the BH&HLYP method is computationally much less expensive than either the MP2 or QCISD methods. The most noticeable discrepancy in the transition state frequencies calculated at different levels of theory is for the unbound mode. The
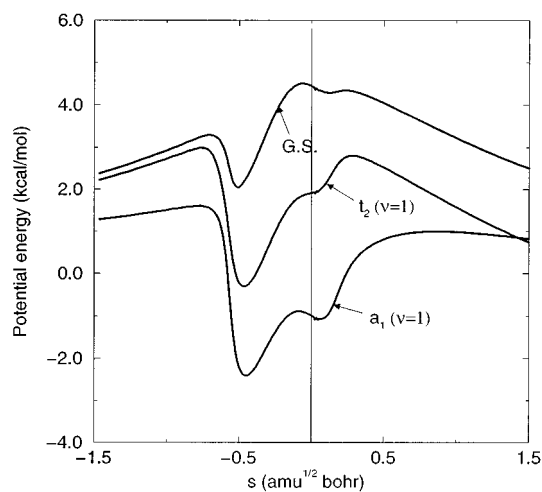

FIG. 2. BH&HLYP/6-311G(d,p) generalized frequencies plotted vs the reaction coordinate s. Diamonds are QCISD/6-311G(d,p) calculated transition state frequencies.

FIG. 4. Top curve is the vibrationally adiabatic ground-state potential energy curve plotted vs the reaction coordinate s. The middle and bottom curves are the vibrationally diabatic curves for exciting the CH_4 umbrella bend (t_2) and symmetric stretch (a_1) modes by one quanta, respectively.

TABLE IV. Calculated and experimental forward rate constants (cm^3 molecule^{-1} s^{-1}) for the CH$_4$+Cl→CH$_3$+HCl reaction.

T (K)	TST	TST/W	CVT	CVT/SCT	CVT/SCT no S.O. coupling[a]	Expt.[b]
200	3.70E-16[c]	1.61E-15	3.24E-16	1.10E-15	3.53E-14	1.11E-14
250	3.37E-15	7.98E-15	3.03E-15	6.64E-15	1.07E-13	4.34E-14
290	1.17E-14	2.37E-14	1.07E-14	1.92E-14	2.10E-13	9.17E-14
300	1.53E-14	2.98E-14	1.40E-14	2.41E-14	2.44E-13	1.01E-13
350	4.69E-14	7.96E-14	4.35E-14	6.49E-14	4.72E-13	2.14E-13
400	1.13E-13	1.73E-13	1.05E-13	1.43E-13	8.13E-13	3.75E-13
450	2.31E-13	3.28E-13	2.17E-13	2.77E-13	1.29E-12	5.81E-13
500	4.21E-13	5.65E-13	3.97E-13	4.84E-13	1.94E-12	8.25E-13
600	1.11E-12	1.37E-12	1.05E-12	1.20E-12	3.83E-12	
800	4.38E-12	4.96E-12	4.15E-12	4.48E-12	1.07E-11	
1000	1.14E-11	1.24E-11	1.08E-11	1.14E-11	2.27E-11	

[a]The spin−orbit coupling effects of the Cl atom were not included.
[b]Taken from Arrhenius fits to experimental data (Ref. 9).
[c]Read as 3.70×10^{-16}.

imaginary frequency, however, depends strongly on the barrier height. The BH&HLYP imaginary frequency is 232 cm^{-1} smaller than the QCISD value. This is partly due to the QCISD classical barrier being too high as will be discussed below.

3. Energetics

Reaction energies and barrier heights calculated using DFT and *ab initio* MO theories are listed in Table III. First, we discuss the reaction energy and enthalpy, ΔE and ΔH, respectively. The calculated reaction energy varies from 6.38 to 9.85 kcal/mol. The BH&HLYP and QCISD results are 2 to 3 kcal/mol more endothermic than the PMP4(SDTQ), MP-SAC2, and CCSD(T) values. The heats of reaction calculated at the PMP4//BH&HLYP, MP-SAC2, and CCSD(T)//MP2 levels are 1.02, 1.2, and 1.91 kcal/mol, respectively. These values are in good agreement with the experimental heat of reaction of 1.89±0.10 kcal/mol. The BH&HLYP and QCISD reaction enthalpies, however, are 1.7 to 2.6 kcal/mol too large. Note that the QCISD method predicts a substantially higher classical forward barrier than other theoretical methods. Adding the zero-point energy correction lowers the forward barrier significantly. In particular, the calculated zero-point energy corrected barriers are 5.54 kcal/mol at the BH&HLYP level, 9.77 at QCISD, 3.55 at PMP4//BH&HLYP, 4.53 at MP4//BH&HLYP, 3.5 at MP-SAC2, and 4.93 at CCSD(T)//MP2 levels of theory. Comparing to the experimental activation energy of 3.5 kcal/mol in the range of 360–500 K, we find that the PMP4//BH&HLYP level of theory used in the present study yields excellent agreement. Such agreement may be due to cancellation between quantum mechanical tunneling effects, which lower the activation energy, and the spin−orbit coupling and recrossing effects, which effectively raise the barrier. The zero-point energy corrected reverse barriers calculated by the BH&HLYP and PMP4//BH&HLYP levels are 0.92 and 1.50 kcal/mol respectively. They are in good agreement with MP-SAC2 and CCSD(T) values of 1.2 and 2.11 kcal/mol, respectively. The QCISD method, however, predicts a substantially higher barrier. The UMP4 barrier heights are about 1 kcal/mol higher

than the PMP4 results. This difference indicates the magnitude of the error in the energy due to the spin contamination in the UMP4 calculations.

In conclusion, although the BH&HLYP/6-311G(d,p) method predicts accurate geometries and frequencies at the stationary points, it still has noticeable errors in calculating the heat of reaction and barrier height for the Cl+CH$_4$ reaction. Single point PMP4(SDTQ) calculations with a much larger 6-311+G($2df$,$2pd$) basis set bring the calculated energetic information into good agreement with experimental data. This is particularly encouraging for direct *ab initio* dynamical calculations of rate constants for this reaction. In particular, by using a combined DFT/MO approach, a sufficiently accurate reaction valley can be obtained with much less computational resource than if it were calculated only from *ab initio* MO theories at the same level of accuracy. The combined DFT/MO approach used here involved using the BH&HLYP/6-311G(d,p) method to calculate the geom-
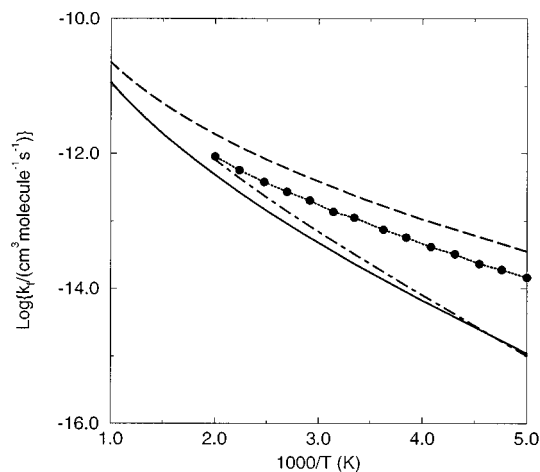

FIG. 5. Calculated and experimental forward rate constants for the CH$_4$+Cl→CH$_3$+HCl reaction plotted vs 1000/T. Dashed line is the CVT/SCT rate constants without the spin−orbit coupling effects. Dotted line is experimental data from an Arrhenius fit (Ref. 9). Solid line is the full CVT/SCT results. Dotted−dashed line is from Dobbs and Dixon (Ref. 17).

TABLE V. Calculated and experimental reverse rate constants (cm^3 molecule^{-1} s^{-1}) of the CH$_4$+Cl↔CH$_3$+HCl reaction.

T (K)	TST	TST/W	CVT	CVT/SCT	Expt.[a]	Expt.[b]
200	2.93E-15[c]	9.19E-15	2.56E-15	8.69E-15		
250	8.59E-15	2.04E-14	7.74E-15	1.69E-14		
290	1.56E-14	3.15E-14	1.43E-14	2.55E-14		
300	1.77E-14	3.45E-14	1.62E-14	2.79E-14	6.59E-14	4.78E-14
350	3.00E-14	5.09E-14	2.78E-14	4.15E-14	1.10E-13	6.68E-14
400	4.52E-14	6.94E-14	4.23E-14	5.75E-14	1.61E-13	8.59E-14
450	6.34E-14	9.02E-14	5.96E-14	7.60E-14	2.17E-13	1.04E-13
500	8.45E-14	1.13E-13	7.98E-14	9.71E-14	2.75E-13	1.22E-13
600	1.36E-13	1.68E-13	1.29E-13	1.48E-13		
800	2.81E-13	3.19E-13	2.66E-13	2.88E-13		
1000	4.94E-13	5.36E-13	4.66E-13	4.90E-13		

[a]From Ref. 14.
[b]From Ref. 3.
[c]Read as 2.93×10^{-15}.

etries and frequencies along the MEP and then performing a series of single point PMP4/6-311+G(2df,2pd) calculations to correct the energy.

B. Minimum energy path

1. Geometries

Geometrical parameters obtained from the BH&HLYP method for points along the MEP are plotted in Fig. 1. The results of our QCISD calculations are referenced as diamonds on Fig. 1. It is interesting to note that as the reaction proceeds to products, the active CH bond undergoes relatively small changes until the reaction coordinates reaches about ~0.6 amu$^{1/2}$ bohr then rapidly dissociates. Similar but less dramatic changes are also observed for the active HCl bond and the H′CH angle. As a technical note, no oscillation in the geometrical parameters was observed when integrating

further to the entrance and exit channels. This indicates that the integration step size used in calculating the MEP is sufficiently small.

2. Frequencies

We have correlated the BH&HLYP generalized frequencies along the MEP as plotted in Fig. 2. For comparison, QCISD transition state frequencies are also plotted in Fig. 2 as diamonds. Rapid decreases of the CH symmetric stretching (a_1 symmetry) and umbrella bending (t_2 symmetry) modes occur at about $s=-0.6$ amu$^{1/2}$ bohr. In particular, the symmetric stretching frequency is about 1/2 of its starting value at the transition state. The umbrella bending mode is about 1/3 of its starting value at the transition state. These large frequency changes will have important consequences in the vibrational-state selected rates for the reaction as discussed below.
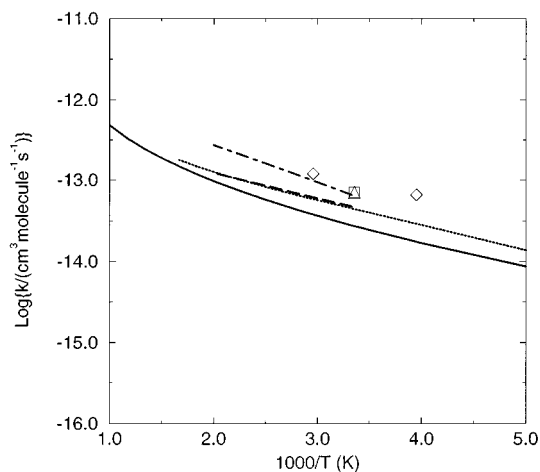

FIG. 6. Calculated and experimental reverse rate constants for the CH$_4$+Cl→CH$_3$+HCl reaction plotted vs 1000/T. Diamonds are from Ref. 11; square—Ref. 8; triangles—Ref. 10. Dashed and dotted–dashed lines are from Arrhenius fits to experimental data from (Ref. 3) and (Ref. 14), respectively. Solid line is our CVT/SCT calculated reaction rate constant. Dotted line is from Chen et al. (Ref. 18)
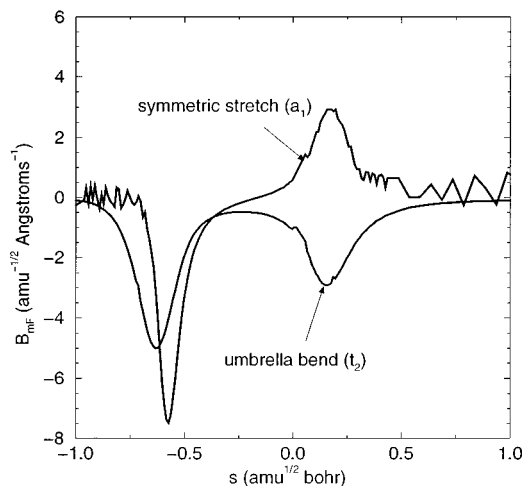

FIG. 7. Vibrational–reaction-coordinate B_{mF} couplings vs the reaction coordinate s.

TABLE VI. Location of variational transition states (amu$^{1/2}$ bohr) for the thermal and vibrational-state selected CH$_4$+Cl→CH$_3$+HCl reaction.

T (K)	Thermal	CH$_4(\nu_{t2}=1)$+Cl	CH$_4(\nu_{a1}=1)$+Cl
200	−0.061	0.283	−0.903
250	−0.061	0.281	−0.903
300	−0.061	0.278	−0.903
400	−0.061	0.256	−0.903
500	−0.061	0.252	−0.903
800	−0.062	0.220	−0.903
1000	−0.076	−0.088	−0.903

3. Energies

The classical potential energy curves along the MEP calculated at both BH&HLYP/6-311G(d,p) and PMP4/6-311+G($2df,2pd$) levels are shown in Fig. 3 and have similar shape, though the BH&HLYP curve has a 2.0 kcal/mol higher barrier. The CCSD(T)//MP2 barrier[17] is also shown by the triangle. The single point PMP4(SDTQ) calculations shift the maximum to the product direction by 0.037 amu$^{1/2}$ bohr. In order to obtain accurate variational effects in rate calculations, we have shifted the PMP4(SDTQ) potential curve so that the maximum occurs at $s=0$.

The vibrationally ground-state adiabatic potential curve is plotted in Fig. 4 along with the diabatic potential curves for exciting by one quanta in either the CH symmetric stretching or umbrella bending mode. In Fig. 4 we have included the spin–orbit coupling effects of the Cl atom,[42] which effectively raises the barrier by 0.84 to 4.39 kcal/mol. Exciting the CH symmetric stretching or umbrella bending mode was found to lower the barrier and thus would significantly enhance the reaction rates. More quantitative discussion on rate constants is given below. Notice that when either the CH symmetric stretching or umbrella bending mode is excited by one quanta the barrier location moves by approximately −0.6 amu$^{1/2}$ bohr toward the entrance channel into the region where drastic changes in geometry and generalized frequencies were observed to begin.

C. Thermal rate constants

1. Forward rate

Calculated thermal rate constants for the CH$_4$+Cl reaction are listed in Table IV. The corresponding Arrhenius plot of both theoretical and experimental rate constants is shown in Fig. 5. Note that for this reaction, a few experimental rate constants (example Refs. 2, 4–7, 10–13) are available for comparison. Results from an Arrhenius fit to a large number of these experimental points[9] were used in Fig. 5. Previous TST/W rate constants[17] are also plotted on Fig. 5. Our CVT/SCT rate constants are noticeably lower than the experimental values by factors increasing from 1.7 to 10 as the temperature decreases from 500 to 200 K. Previous theoretical work,[17] which did not include spin–orbit effects, yielded slightly better agreement with experiment at high temperatures. The small difference between CVT and TST rates implies that recrossing effects have a small effect on the reaction dynamics. To illustrate the spin–orbit coupling effects on the rate, we also plot the calculated CVT/SCT rate constants when these effects were not included. In this case, cancellation of tunneling and spin–orbit coupling effects give better agreement with experimental results.

The differences between the present results and experimental data are due to two sources. One is that the small-curvature (SCT) tunneling approximation is known to underestimate the tunneling contribution for $\mathcal{H}$–$\mathcal{L}$–$\mathcal{H}$ reactions. This perhaps is the largest source of error in our calculated rate constants particularly at low temperatures. Note that Wigner tunneling corrections are comparable to the small-curvature tunneling correction results. The present results indicate that one needs to perform large curvature tunneling (LCT) calculations to obtain more accuracy. Unfortunately, full LCT calculations within the direct *ab initio* dynamics approach employed here are still computationally unfeasible. An approximate LCT method is being developed in our lab. At higher temperatures our results get progressively better agreement with experimental data, as tunneling becomes less important. The second source is perhaps due to the calculated potential width being too large as indicated by the

TABLE VII. Calculated vibrational-state selected forward rate constants (cm^3 molecule^{-1} s^{-1}) for the CH$_4$+Cl→CH$_3$+HCl reaction.

| T (K)	CH$_4(\nu_{t2}=1)$+Cl			CH$_4(\nu_{a1}=1)$+Cl	
	TST	CVT	CVT/SCT	TST	CVT
200	2.12E-13[a]	2.55E-14	5.72E-14	3.13E-10	1.77E-12
250	5.23E-13	1.03E-13	1.72E-13	1.86E-10	3.99E-12
290	8.76E-13	2.30E-13	3.35E-13	1.43E-10	6.28E-12
300	9.78E-13	2.72E-13	3.88E-13	1.36E-10	6.90E-12
350	1.57E-12	5.62E-13	7.29E-13	1.14E-10	1.03E-11
400	2.30E-12	9.98E-13	1.22E-12	1.02E-10	1.39E-11
450	3.18E-12	1.61E-12	1.88E-12	9.74E-11	1.78E-11
500	4.20E-12	2.40E-12	2.73E-12	9.59E-11	2.17E-11
600	6.74E-12	4.65E-12	5.08E-12	9.91E-11	2.97E-11
800	1.40E-11	1.21E-11	1.27E-11	1.18E-10	4.57E-11
1000	2.44E-11	2.30E-11	2.38E-11	1.31E-10	6.10E-11

[a]Read as 2.12×10^{-13}.
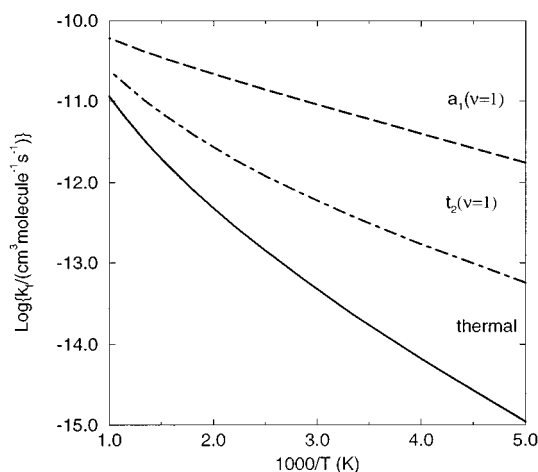
FIG. 8. Calculated CVT/SCT vibrational-state selected rate constants for the CH$_4$+Cl→CH$_3$+HCl reaction plotted vs $1000/T$ (K). Dashed line is for exciting the CH$_4$ symmetric stretch mode by one quanta and dotted–dashed line is for exciting the CH$_4$ umbrella bend mode by one quanta. Solid line is from CVT/SCT thermal rate constants.
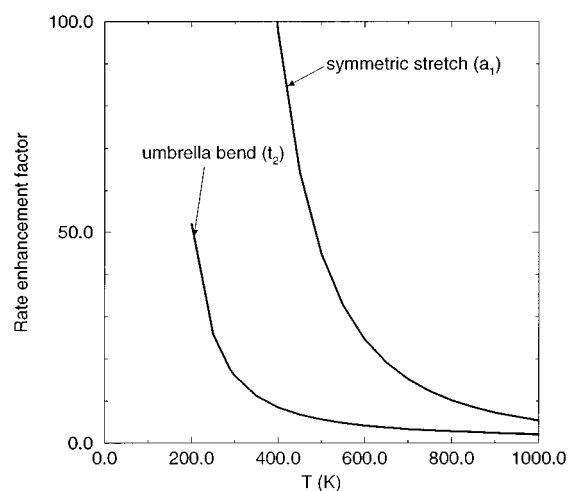

FIG. 9. Plot of enhancement factors vs the temperature T for the vibrational-state selected rates for excitation of either the CH$_4$ symmetric stretch or umbrella bend mode.

BH&HLYP imaginary frequency being too small (see Table II). Furthermore, the effects of anharmonicity were not included in this study. Anharmonicity was found to lower the thermal rate constants for the similar CH$_4$+H↔CH$_3$+H$_2$ reaction by 60% at 667 K.[55]

2. Reverse rate

The experimental and calculated CVT/SCT rate constants for the CH$_3$+HCl reaction are listed in Table V and the corresponding Arrhenius plot is shown in Fig. 6. There is a limited amount of experimental data available for this reaction with a correspondingly larger degree of uncertainty.[3,8,10,11,14] A recent work by Russel et al. is probably the most accurate because more direct detection techniques were used. We found that rate constants measured by Russel et al.[3] are larger than our calculated CVT/SCT results by a factor increasing from 1.3 to 1.7 as the temperature decreases from 500 to 300 K. Previously calculated rate constants[18] based on RRKM theory are also shown on Fig. 6 and show better agreement with experiments. For the reverse reaction, we also found that recrossing effects in the thermal rate are small as indicated by small difference in TST and CVT results. Tunneling contributions calculated from the SCT approximation were found to enhance the thermal rate by a factor increasing from 1.05 to 3.39 as the temperature

decreases from 1000 to 200 K. Such factors are expected to be too small due to the same reason discussed above.

D. Vibrational-state selected rate constants

The B_{mF} couplings between the vibrational modes and the reaction coordinate motion as functions of the reaction coordinate are shown in Fig. 7 for the C–H symmetric stretch and umbrella bending modes of methane. Other vibrational modes have small coupling to the reaction coordinate, thus need not be discussed here. The large B_{mF} couplings for the CH$_4$ umbrella bend and symmetric stretch modes indicate that excitation of these modes would greatly enhance the reaction rates.[56–58] Notice that large B_{mF} coupling occurs in regions where the generalized frequencies and geometries as functions of the reaction coordinate have large curvatures.

The effects of exciting either the CH symmetric stretch (a_1) or umbrella bend (t_2) mode can be seen qualitatively from the diabatic potential energy curves shown in Fig. 4. In particular, exciting the CH symmetric stretch or the umbrella bend by one quanta effectively lowers the barrier to 1.62 and 3.55 kcal/mol, respectively as compared to the zero-point energy corrected barrier of 3.55 kcal/mol (see Table III) for the CH$_4$+Cl reaction. For the reverse CH$_3$+HCl reaction, vibrational excitation of the HCl molecule effectively re-

TABLE VIII. Rate enhancement factors for the CH$_4$+Cl→CH$_3$+HCl reaction resulting from excitation of the umbrella bend (t_2) or the symmetric stretch (a_1) of CH$_4$ by one quanta.

T (K)	CH$_4(\nu_{t2}=1)$+Cl	CH$_4(\nu_{a1}=1)$+Cl
200	52	1600
300	16	290
500	5.6	45
800	2.8	10
1000	2.1	5.4

TABLE IX. Total energies (hartree).

	BH&HLYP[a]	QCISD[a]	PMP4//DFT[b]
Cl	−460.1546	−459.6017	−459.6585
HCl	−460.8136	−460.2603	−460.3249
CH$_3$	−39.8241	−39.7292	−39.7600
CH$_4$	−40.4973	−40.4016	−40.4366
H$_3$C···H···Cl	−500.6362	−499.9828	−500.0826
H$_3$C···HCl complex	−500.6414	−499.9923	−500.0886

[a]Calculated using the 6-311G(d,p) basis set.
[b]Single point PMP4/6-311+G($2df$,$2pd$) energy calculation at the BH&HLYP/6-311G(d,p) geometries.

moves the barrier to hydrogen atom transfer. A more interesting result is that exciting the CH$_3$ umbrella bend effectively raises the barrier to 3.68 kcal/mol which is 1.53 kcal/mol above the zero-point energy corrected barrier (see Table III). Thus, qualitatively, the present results predict that vibrational excitation of the umbrella bending mode will have opposite effects on the forward and reverse rates of the CH$_4$+Cl↔CH$_3$+HCl reaction. Experimental study on such effects for the reverse reaction would be difficult, however, due to the high reactivity of methyl radicals toward the recombination process.

There are significant changes in the shapes of the potential energy curves due to excitation of these two methane vibrational modes. Of particular interest is the shift in the position of the temperature-dependent vibrational transition states as listed in Table VI. We found that for the CH$_4$(ν_{a1}=1)+Cl reaction the canonical variational transition states are located at s about −0.90 amu$^{1/2}$ bohr and are not strongly dependent on temperature. In contrary, as the temperature increases from 200 to 1000 K, the location of the CVT bottleneck for the CH$_4$(ν_{t2}=1)+Cl reaction shifts from s equal to 0.28 to −0.09 amu$^{1/2}$ bohr and thus exhibits small temperature dependence. Such large shifts in the dynamical bottlenecks indicate that conventional TST theory will overestimate vibrational-state selected rates of this reaction as discussed more below.

The calculated vibrational-state selected forward rate constants using the statistical adiabatic model described earlier are listed in Table VII and the corresponding Arrhenius plot is shown in Fig. 8. First, we discuss the rates of the CH$_4$(ν_{a1}=1)+Cl reaction. Since the diabatic potential curve for this reaction is nearly barrierless (see Fig. 4), tunneling contributions are not calculated in this case. Note that the diabatic model does not include contributions from tunneling to the ground-state products. As mentioned above, the temperature-dependent CVT transition states shift significantly to the reactant channel. As a consequence, TST overestimates the rate constant, for instance, by a factor of 20 at 300 K. There is a significant enhancement of the reaction rate due to excitation of the CH$_4$ symmetric stretch mode. Enhancement factors, which are ratios of the vibrational-state selected and thermal rate constants, are listed in Table VIII and shown in Fig. 9. In particular, at room temperature, the enhancement factor is on the order of 300. A more interesting result is the effect of exciting the CH$_4$ umbrella bend mode on the rate. This mode has low frequency and does not directly participate in the bond breaking or forming process, thus it would be expected to have negligible effect on the rate. However, since its equilibrium value changes from the sp^3 tetrahedral to planar sp^2 angle as the reaction proceeds from the reactants to products, one can expect some coupling between the umbrella bend mode and the reaction coordinate. In fact, the enhancement factor for exciting the umbrella bending mode (t_2) by one quanta is on the order of 20 at room temperature.

Finally, it is important to access the accuracy of different approximations used in this study and how it affects the numerical results.

(a) The use of TST method, as mentioned earlier, due to the significant shifts in the dynamical bottleneck in the vibrational-state selected rates, will significantly overestimate the rate. CVT theory is preferred in this case since it can approximately locate such a bottleneck by variationally minimizing the rate along the reaction coordinate.

(b) We have used the SCT method to estimate tunneling contributions. It is known that the SCT method often underestimates the tunneling probability for $\mathscr{H}-\mathscr{L}-\mathscr{H}$ reactions. Since the barriers for the vibrational-state selected reactions considered here are lower than for the thermal case, we can expect such underestimation is more severe in calculation of thermal rates. As a consequence, the calculated enhancement factors due to excitation of either the CH symmetric stretch or umbrella bend mode should be smaller. We are now in the process of developing a more accurate tunneling method, namely a LCT method, that can be used with our direct *ab initio* dynamics approach.

(c) The statistical diabatic model used in this study to calculate vibrational-state selected rates is an approximate model and should be viewed as such. This model assumes that vibrational modes preserve their characteristic motions along the reaction coordinate and does not account for vibration-to-vibration energy transfer. Therefore, it is expected to work well for vibrational-state selected reactions where the dynamical bottleneck is located early in the entrance channel, such as the CH$_4$(ν_{a1}=1)+Cl reaction in this study.

V. CONCLUSION

We have performed a direct *ab initio* dynamics study on the thermal and vibrational-state selected rates of the CH$_4$+Cl↔CH$_3$+HCl reaction. This is in fact the first detailed analysis on the reaction valley as well as vibrational-state specific chemistry of this reaction. Due to the size of the system, i.e., the total number of electrons, we have used our previously proposed combined DFT/MO approach to obtain the potential energy surface information needed for rate calculations. In fact, we found that the BH&HLYP method with the 6-311G(d,p) basis set yields geometries and frequencies at the stationary points of comparable accuracy to the more computationally expensive QCISD/6-311G(d,p) level. Therefore, we used the BH&HLYP/6-311G(d,p) method to calculate geometries and generalized frequencies along the reaction coordinate. (See Table IX.) More accurate barrier height and width were obtained by performing a series of PMP4(SDTQ) single point calculations with a much larger 6-311+G($2df$,$2pd$) basis set.

Thermal rate constants were calculated for a wide range of temperatures using a *full* CVT theory augmented by a multidimensional semiclassical SCT correction for both the forward and reverse directions of the CH$_4$+Cl↔CH$_3$+HCl reaction. The spin−orbit coupling effect was also included for the forward reaction. Note that no experimental data other than physical constants was used in this study. We found that our calculated thermal rate constants are smaller

than the experimental measurements by at most an order of magnitude, particularly at low temperatures. We attributed such differences to the error in the SCT method for estimating the tunneling probability.

Finally, we have used a statistical diabatic model to provide a qualitative analysis on the possible vibrational-state specific chemistry of this reaction. In fact, we found that there are strong couplings between the CH$_4$ symmetric stretch and umbrella bend modes with the reaction coordinate. This indicates that excitations of these modes would enhance the reaction rates. We have estimated such enhancement factors and found that exciting the CH$_4$ symmetric stretch mode significantly enhances the rate, for instance, by a factor of 300 at room temperature, whereas exciting the CH$_4$ umbrella bend mode has a noticeable (perhaps measurable) enhancement. For the reverse CH$_3$+HCl reaction, due to the possible difficulty in experimental verification, we provide only a qualitative discussion on the effects of vibrational excitation of either the HCl stretch or CH$_3$ umbrella bend on the dynamics of this reaction. In particular, we predicted that exciting the HCl stretch mode would enhance the rate whereas exciting the CH$_3$ umbrella bend mode would have the opposite effect. We hope this study will motivate experimental verification.

Although the present study provides the most detailed description on the dynamics of the CH$_4$+Cl↔CH$_3$+HCl reaction to date, much more work is still needed to achieve the desired accuracy. We are taking steps in this direction.

ACKNOWLEDGMENTS

[1] F. S. Rowland and M. J. Molina, Rev. Geophys. Space Phys. **13**, 1 (1975).
[2] A. R. Ravishankara and P. H. Wine, J. Chem. Phys. **72**, 25 (1980).
[3] J. J. Russel, J. A. Seetula, S. M. Senkan, and D. Gutman, Int. J. Chem. Kin. **20**, 759 (1988).
[4] J.-P. Sawerysyn, C. Lafage, B. Meriaux, and A. Tighezza, J. Chim. Phys. **84** (1987).
[5] W. R. Simpson, A. J. Orr-Ewing, and R. N. Zare, Chem. Phys. Lett. **212**, 1963 (1993).
[6] D. A. Whytock, J. Chem. Phys. **66**, 2690 (1977).
[7] M. S. Zahniser, B. M. Berquist, and F. Kaufman, Int. J. Chem. Kin. **10** (1978).
[8] M. H. Baghal-Vayjooee, J. Am. Chem. Soc. **100**, 3214 (1978).
[9] W. B. DeMore, S. P. Sander, D. M. Golden, R. F. Hampson, M. J. Kurylo, C. J. Howard, A. R. Ravishankara, C. E. Kolb, and M. J. Molina, in *JPL publication 92-20* (Jet Propulsion Laboratory, Pasadena, CA, 1992).
[10] O. Dobis and S. W. Benson, Int. J. Chem. Kin. **19**, 691 (1987).
[11] S. P. Heneghan, P. A. Knoot, and S. W. Benson, Int. J. Chem. Kin. **13**, 677 (1981).
[12] L. F. Keyser, J. Chem. Phys. **69**, 214 (1978).
[13] C. L. Lin, M. T. Leu, and W. B. DeMore, J. Phys. Chem. **82** (1978).
[14] M.-L. Pohjonen and J. Koskikallio, Acta Chemica Scandinavica A **33**, 449 (1979).
[15] T. N. Truong and D. G. Truhlar, J. Chem. Phys. **90**, 7137 (1989).
[16] Y. Chen, E. Tschuikow-Roux, and A. Rauk, J. Phys. Chem. **95**, 9832 (1991).
[17] K. D. Dobbs and D. A. Dixon, J. Phys. Chem. **98**, 12584 (1994).
[18] Y. Chen, A. Rauk, and E. Tschuikow-Roux, J. Phys. Chem. **95**, 9900 (1991).
[19] E. Wigner, J. Chem. Phys. **5**, 720 (1937).
[20] A. Gonzalez-Lafont, T. N. Truong, and D. G. Truhlar, J. Chem. Phys. **95**, 8875 (1991).
[21] A. D. Becke, Phys. Rev. A **38**, 3098 (1988).
[22] A. D. Becke, J. Chem. Phys. **98**, 5648 (1993).
[23] C. Lee, W. Yang, and R. G. Parr, Phys. Rev. B **37**, 785 (1988).
[24] T. N. Truong and W. Duncan, J. Chem. Phys. **101**, 7408 (1994).
[25] R. L. Bell and T. N. Truong, J. Chem. Phys. **101**, 10442 (1994).
[26] T. N. Truong, J. Chem. Phys. **102**, 5335 (1995).
[27] A. D. Becke, J. Chem. Phys. **98**, 1372 (1993).
[28] J. J. Valentini, P. M. Aker, G. J. Germann, and Y.-D. Huh, Faraday Discuss. Chem. Soc. **91**, 173 (1991).
[29] B. Amaee, J. N. L. Connor, and J. C. Whitehead, Faraday Discuss. Chem. Soc. **84**, 387 (1987).
[30] J. C. Polanyi, Acc. Chem. Res. **5**, 161 (1972).
[31] W. R. Simpson, A. J. Orr-Ewing, and R. N. Zare, Chem. Phys. Lett. **212**, 163 (1993).
[32] S. C. Tucker and D. G. Truhlar, in *New Theoretical Concepts For Understanding Organic Reactions*, edited by J. Bertran and I. G. Csizmadia (Kluwer, Dordrecht, The Netherlands, 1989), pp. 291–346.
[33] A. Gonzalez-Lafont, T. N. Truong, and D. G. Truhlar, J. Phys. Chem. **95**, 4618 (1991).
[34] A. A. Viggiano, J. Paschekewitz, R. A. Morris, J. F. Paulson, A. Gonzalez-Lafont, and D. G. Truhlar, J. Am. Chem. Soc. **113**, 9404 (1991).
[35] Y.-P. Liu, G. C. Lynch, T. N. Truong, D.-h. Lu, and D. G. Truhlar, J. Am. Chem. Soc. **115**, 2408 (1993).
[36] Y.-P. Liu, D.-h. Lu, A. Gonzalez-Lafont, D. G. Truhlar, and B. C. Garrett, J. Am. Chem. Soc. **115**, 7806 (1993).
[37] W.-P. Hu, Y.-P. Liu, and D. G. Truhlar, J. Chem. Soc. Faraday Trans. **90**, 1715 (1994).
[38] D. G. Truhlar and B. C. Garrett, Annu. Rev. Phys. Chem. **35**, 159 (1984).
[39] D. G. Truhlar, A. D. Isaacson, and B. C. Garrett, in *Theory of Chemical Reaction Dynamics*, Vol. 4, edited by M. Baer (CRC, Boca Raton, FL, 1985), pp. 65–137.
[40] D.-h. Lu, T. N. Truong, V. S. Melissas, G. C. Lynch, Y. P. Liu, B. C. Garrett, R. Steckler, A. D. Isaacson, S. N. Rai, G. C. Hancock, J. G. Lauderdale, T. Joseph, and D. G. Truhlar, Comput. Phys. Comm. **71**, 235 (1992).
[41] D. G. Truhlar and A. D. Isaacson, J. Chem. Phys. **77**, 3516 (1982).
[42] G. C. Schatz, J. Phys. Chem. **99**, 7522 (1995).
[43] R. S. Grev and H. F. I. Schaefer, J. Chem. Phys. **91**, 7305 (1989).
[44] T. H. Dunning, Jr., J. Chem. Phys. **90**, 1007 (1989).
[45] R. A. Kendall, T. H. Dunning, Jr., and R. J. Harrison, J. Chem. Phys. **96**, 6796 (1992).
[46] D. E. Woon and T. H. Dunning, Jr., J. Phys. Chem. **98**, 1358 (1993).
[47] GAUSSIAN 92/DFT, Revision G.3, M. J. Frisch, G. W. Trucks, H. B. Schlegel, P. M. W. Gill, B. G. Johnson, M. W. Wong, J. B. Foresman, M. A. Robb, M. Head-Gordon, E. S. Replogle, R. Gomperts, J. L. Andres, K. Raghavachari, J. S. Binkley, C. Gonzalez, R. L. Martin, D. J. Fox, D. J. Defrees, J. Baker, J. J. P. Stewart, and J. A. Pople (Gaussian, Inc., Pittsburgh, 1993).
[48] J. Baker, J. Andzelm, M. Muir, and P. R. Taylor, Chem. Phys. Lett. **237**, 53 (1995).
[49] C. Gonzalez and H. B. Schlegel, J. Phys. Chem. **94**, 5523 (1990).
[50] H. B. Schlegel, J. Phys. Chem. **92**, 3075 (1988).
[51] K. Krishnan and J. A. Pople, Int. J. Quant. Chem. **14**, 91 (1978).
[52] T. N. Truong, J. Chem. Phys. **100**, 8014 (1994).
[53] T. N. Truong, DiRate (unpublished), Revision 1.0 (University of Utah, Salt Lake City, 1993).
[54] *JANAF Thermochemical Tables*, Vol. 37, edited by D. R. Stull and H. Prophet (Natl. Stand, Ref. Data Ser., Natl. Bur. Stand, Washington, DC, 1971).
[55] T. Joseph, B. C. Garrett, and D. G. Truhlar, J. Chem. Phys. **88**, 6982 (1988).
[56] T. H. Dunning, R. A. Bair, R. A. Eades, L. B. Harding, and R. L. Shepard, J. Phys. Chem. **90**, 344 (1986).
[57] T. H. Dunning, R. A. Eades, and E. Kraka, Faraday Discuss. Chem. Soc. **427** (1987).
[58] T. H. Dunning, J. M. Bowman, G. C. Schatz, A. F. Wagner, and L. B. Harding, Science **240**, 453 (1988).